Evaluating Sugar Signaling during Xylose Oxidation in *Saccharomyces cerevisiae*

A Master Thesis at the Division for Applied Microbiology,
Faculty of Engineering at Lund University

Spring 2020

LUND UNIVERSITY

LTH
FACULTY OF ENGINEERING

Principle Supervisor: Marie Gorwa-Grauslund

Laboratory Supervisor: Celina Borgström

Examiner: Ed van Niel

By Viktor Persson

Table of Contents

Abstract

The sugar signaling state of cells oxidizing xylose was investigated through the chromosomal integration of the Weimberg pathway into previously established biosensor strains capable of monitoring the Snf3p/Rgt2p, SNF1/Mig1p, and cAMP/PKA pathways through the expression of *HXT1*, *SUC2*, and *TPS1*, respectively. Ultimately, two new strains were successfully developed containing both the Weimberg pathway and a biosensor for either *HXT1* (TMB CB 112) or *TPS1* (TMB CB 117). Unfortunately, the *SUC2*-based Weimberg biosensor (TMB CB 115) showed impaired growth and seemingly lacked a diauxic shift, making it unable to assimilate xylose. As for xylose utilization, the working Weimberg biosensor strains showed xylose assimilation rates similar to the benchmark Weimberg pathway strain (TMB4586), which remained lower than that of the oxidoreductase pathway biosensor strains (TMB375X series). Aside from the difference in xylose assimilation, the growing Weimberg biosensor strains showed very similar metabolite profiles to both the reference Weimberg pathway strain (TMB4586) and the oxidoreductase biosensor strains (TMB375X series). A signaling assay over a 54-hour cultivation showed clear similarities between the Weimberg biosensors (TMB CB 112, TMB CB 117) and the oxidoreductase biosensors (TMB375X series), and the induction of *SUC2* after glucose depletion indicated that the full “low glucose” signal may only arise once xylose begins being actively metabolized. Finally, a separate 6-hour cultivation was performed in different key media of interest. Interestingly, the Weimberg biosensor strains showed decreased bimodalities similar to the decrease seen after integration of the oxidoreductase pathway in the TMB375X series, indicating that integration of the Weimberg pathway may have a similar effect.

Background

With growing environmental concerns and dwindling fossil fuel reserves, the need for alternative sustainable feedstocks to replace petroleum-based processes has become increasingly apparent [1, 2]. One such feedstock of particular interest is lignocellulose, a composite material of primarily three polymers (cellulose, hemicellulose, and lignin) and a by-product of agriculture and forestry that is already a common substrate in biorefineries [2, 3]. In recent years, lignocellulosic hydrolysates have been recognized as an excellent starting point for the production of chemicals and biofuels through fermentation [4]. Past applications of fermentation on lignocellulosic hydrolysates have been carried out in the industry-favored yeast *Saccharomyces cerevisiae* due to its well-known cultivation characteristics, the wide availability of genetic engineering tools, and its tolerance to the harsh conditions associated with the hydrolysate [4, 5]. Unfortunately, *S. cerevisiae* is not naturally capable of assimilating xylose, which constitutes up to one-third of all sugars found in lignocellulosic hydrolysates [6, 7]. Consequently, many attempts have been made to enable xylose assimilation in *S. cerevisiae*.

Past attempts have typically focused on the introduction of exogenous pathways to accomplish efficient xylose consumption [8-11]. Four exogenous pathways of particular note have been implemented in *S. cerevisiae*: (i) the isomerase pathway, (ii) the oxidoreductase pathway, (iii) the Dahms pathway, and (iv) the Weimberg pathway [9, 10, 12]. In the former two pathways, xylose is converted to xylulose either directly in the case of the isomerase pathway or through xylitol in the case of the oxidoreductase pathway [8], see Figure 1b. Once xylulose has been formed, it is phosphorylated and funneled through the endogenous non-oxidative pentose phosphate pathway into the lower glycolysis for use in either biomass or product formation [8], see Figure 1de. In both the Dahms pathway and the Weimberg pathway, the xylose is instead converted to 2-keto-3-deoxy-xylonate (KDX) through xylonolactone and xylonate, see Figure 1c. In the case of Dahms pathway, the KDX is then used to directly form glycolaldehyde and pyruvate, while in the Weimberg pathway it is used to form cytosolic α-ketoglutarate via the intermediate α-ketoglutarate-semialdehyde. The cytosolic α-ketoglutarate can subsequently either be used for the formation of other dicarboxylic acids or be imported into the mitochondria and used in the central cellular metabolism via the tricarboxylic acid (TCA) cycle to support growth, see Figure 1af [8, 12]. While the isomerase pathway, the oxidoreductase pathway, and the Dahms pathway were primarily expressed to enable bioethanol production via the glycolysis, the Weimberg pathway presents an approach towards the production of dicarboxylic acids without the typical carbon loss associated with the formation of acetyl-CoA from pyruvate [8].

While attempting to develop a xylose assimilating CEN.PK 113-7D *S. cerevisiae* strain by introducing the Weimberg pathway from the freshwater bacterium *Caulobacter crescentus*, Wasserstrom and colleagues found that nearly all xylose was converted to xylonate rather than being fully metabolized [12]. The implementation of the Weimberg pathway was achieved through the chromosomal integration of genes encoding xylose dehydrogenase (XylB), xylonate dehydratase (XylD), 2-keto-3-deoxyxylonate dehydratase (XylX), and α-ketoglutarate semialdehyde dehydrogenase (XylA) from *C. crescentus* [12]. The integration was designed to result in the deletion of *GRE3*, an endogenous xylose reductase gene, in order to increase Weimberg flux [12]. In a subsequent study, Borgström et al. introduced three additional modifications in an effort to enable growth on xylose. Firstly, an endogenous iron metabolism repressor encoded by *FRA2* was deleted in order to facilitate iron-sulfur (Fe-S) cluster loading into the XylD enzyme for increased catalytic activity, as was previously shown by Toivari and colleagues while establishing a functional Dahms

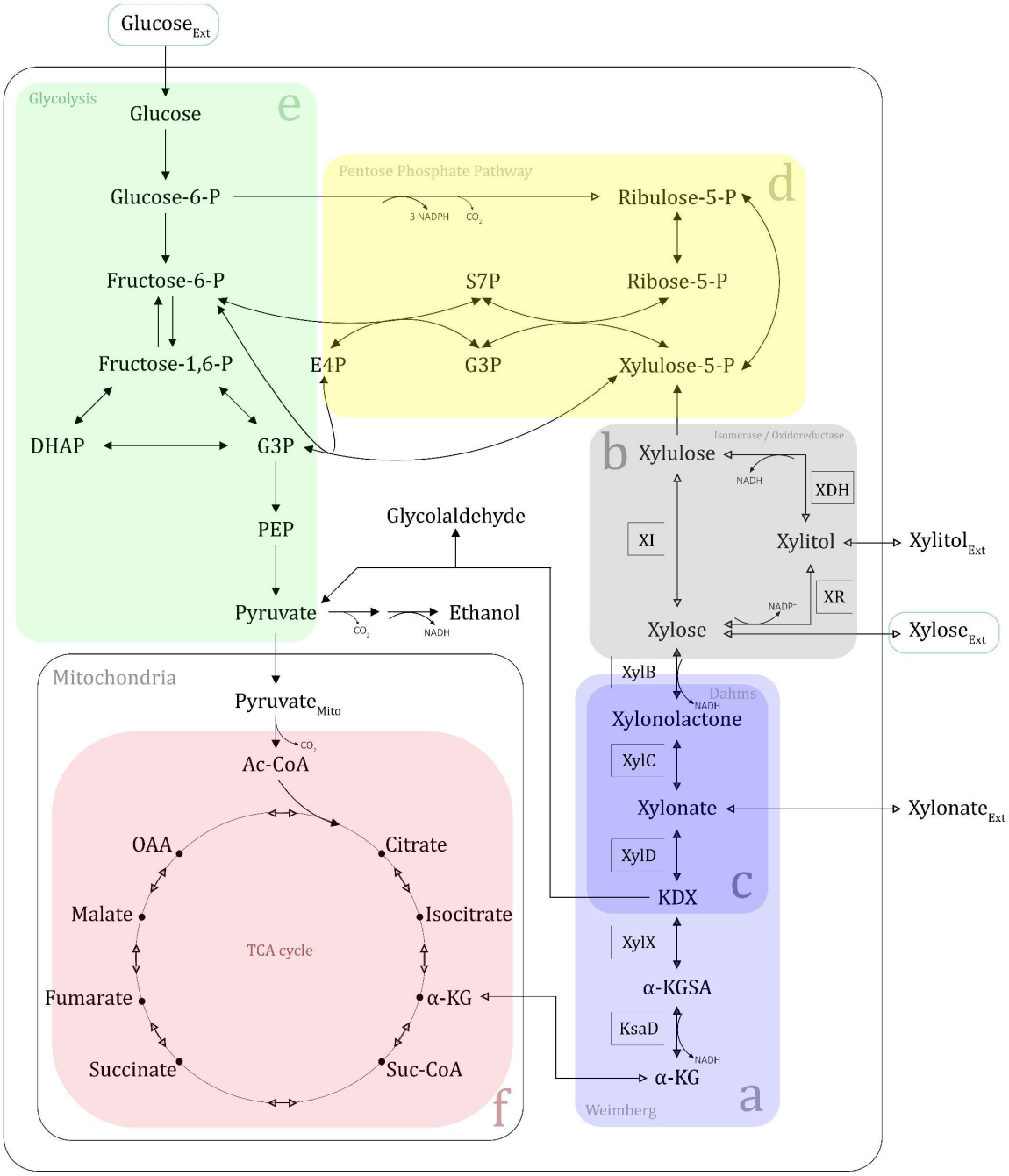

Figure 1. Metabolic map of the Weimberg pathway (light blue, labeled a) in relation to the central carbon metabolism of S. cerevisiae, *adapted from Borgström et al. 2019. Also shown: the isomerase and oxidoreductase pathways (gray, labeled b), Dahms pathway (dark blue, labeled c), the pentose phosphate pathway (yellow, labeled d), the glycolysis (green, labeled e), and the TCA cycle (red, labeled f). The Weimberg pathway is catalyzed by xylose dehydrogenase (XylB), xylonate dehydratase (XylD), 2-keto-3-deoxy-xylonate dehydratase (XylX) and α-ketoglutarate semialdehyde dehydrogenase (KsaD). Finally, the cytosolic α-KG enters the TCA cycle (red) after entering the mitochondria. Abbreviations: α-KG, α-ketoglutaric acid; α-KGSA, α-ketoglutarate semialdehyde; Ac-CoA, Acetyl-Coenzyme A; DHAP, Dihydroxyacetone phosphate; E4P, Erythrose-4-phosphate; G3P, Glyceraldehyde 3-phosphate; KDX, 2-keto-3-deoxy-xylonate; OAA, Oxaloacetic acid; PEP, Phosphoenolpyruvate; S7P, Sedoheptulose-7-phosphate; Suc-CoA, Succinyl-Coenzyme A; TCA cycle, Tricarboxylic acid cycle; XR, Xylose reductase; XDH, Xylitol dehydrogenase; XI, Xylose isomerase.*

pathway in *S. cerevisiae* [8, 12]. Secondly, the last gene of the Weimberg pathway (*xylA*) was replaced with a functional homolog from *Corynebacterium glutamicum* (*ksaD*), resulting in a strain designated TMB4586 which still only produced xylonate [8]. Finally, the three last genes of the pathway (*xylD, xylX, ksaD*) were further overexpressed by introducing three additional copies of each [8]. The final strain, named TMB4590 *(Δgre3, Δfra2, xylB, 4x(xylD, xylX, ksaD)),* produced half as much xylonate as TMB4586 *(Δgre3, Δfra2, xylB, 1x(xylD, xylX, ksaD)* and had a 57% conversion rate through the Weimberg pathway which enabled growth on xylose [8].

A challenge identified in previous xylose assimilating *S. cerevisiae* strains is the lack of co-fermentation, as the yeast preferentially consumes glucose before it begins consuming the xylose [13, 14]. The lack of co-fermentation has been attributed to the absence of xylose-specific transporters, catabolite repression of other carbon sources by the favored glucose, and/or failure to recognize xylose as a fermentable sugar in the signaling of the cell [13, 14]. In order to investigate this issue, biosensor strains with a chromosomally integrated yeast green fluorescent protein gene (*yEGFP3*) linked to key promoters inducible through the *S. cerevisiae* sugar signaling were developed [13]. The chosen promoters, *HXT1/2/4*p, *SUC2*p/*CAT8*p, and *TPS1/2*p, enabled the monitoring of the Snf3p/Rgt2p, SNF1/Mig1p, and cAMP/PKA signaling pathways, respectively [13]. These three cross-talking pathways are key to the sugar signaling seen in *S. cerevisiae* cells, and each recognize different conditions in the cell: (i) the Snf3p/Rgt2p pathway primarily responds to extracellular hexoses and induces the expression of hexose transporter genes such as *HXT1*, *HXT2* and *HXT4*, (ii) the SNF1/Mig1p pathway senses internalized glucose and causes either alternative carbon assimilation during glucose depletion or catabolite repression when intracellular glucose is present, eventually repressing *SUC2* and *CAT8*, (iii) the cAMP/PKA pathway, monitored through expression of the *TPS1/2* promoters, regulates stress responses, the cell cycle, homeostasis, and gluconeogenesis through both Ras1/2p and Gpr1p/Gpa2p which recognize metabolized and extracellular glucose, respectively [13]. The strains were developed from the W303-1A *S. cerevisiae* strain as this background strain had been shown to have intact signaling pathways [15] as opposed to the CEN.PK113-7D strain which contains mutations in the cAMP/PKA pathway [16]. In short, Brink et al. found that *S. cerevisiae* lacked a signaling response to extracellular xylose [13]. In a follow-up study with xylose-engineered strains, Osiro and colleagues demonstrated a distinct signaling response to internalized xylose after enabling uptake through a mutated galactose transporter (*GAL2-N376F*) with xylose affinity (TMB372X series), and further differences were observed when the oxidoreductase pathway was added to enable xylose metabolism (TMB375X series) [14]. Specifically, they found that intracellular xylose gives rise to a similar signal as carbon limitation, i.e. cells grown on high xylose concentrations (50 g/L) had similar signaling to those grown on low glucose (5 g/L). However, it still remained unclear whether the changes to signaling observed were caused by the xylose being present intracellularly, the xylose being metabolized, or the glycolytic intermediates formed as xylose derivatives from the oxidoreductase pathway entered the glycolysis through the non-oxidative pentose phosphate pathway.

In the present study, we implemented the modifications previously introduced in the CEN.PK-based TMB4586 *(Δgre3, Δfra2, xylB, 1x(xylD, xylX, ksaD))* for xylose utilization via the Weimberg pathway in the three W303-based biosensor platform strains TMB3722 (*HXT1p-yEGFP, GAL2-N376F*), TMB3725 (*SUC2p-yEGFP, GAL2-N376F*), and TMB3727 (*TPS1p-yEGFP, GAL2-N376F*), in order to study the effects on sugar signaling caused by xylose metabolism without the formation of glycolytic intermediates.

Results and discussion

Expression of the Weimberg pathway in biosensor strains

The Weimberg pathway used in the present study has previously been expressed in *S. cerevisiae* in two CEN.PK-based strains, TMB4586 (*Δgre3, Δfra2, xylB, 1x(xylD, xylX, ksaD)*) which prominently produced xylonate from xylose and TMB4590 (*Δgre3, Δfra2, xylB, 4x(xylD, xylX, ksaD)*) which displayed sustained growth on xylose in bioreactors [8]. In order to investigate the sugar signaling state of the xylonate-producing TMB4586 strain, the Weimberg pathway was integrated into the W303-based biosensor strains TMB3722, TMB3725, and TMB3727 which report on the expression of the *HXT1*, *SUC2*, and *TPS1* genes, respectively, using green fluorescent protein (GFP).

A CRISPR-Cas9 approach was chosen for the gene integrations to avoid the use of marker-based systems [17]. After the addition of an episomal plasmid carrying the Cas9 recombinase gene (pCfB2312), a single copy of the lower Weimberg pathway genes (*xylD, xylX, ksaD*) were integrated into the chromosomal locus of the *GRE3* gene using a guide RNA (gRNA) from a previous study by Wasserstrom et al. (pLWA25) [12]. Integration of the lower pathway genes thus also led to the simultaneous deletion of the endogenous xylose reductase gene *GRE3*. Similarly, the endogenous iron metabolism repression gene *FRA2* was deleted through the integration of the first Weimberg pathway gene (*xylB*). The *FRA2* locus integration had not previously been performed with the CRISPR-Cas9 system and thus necessitated the design of a novel gRNA (pVP02) which proved successful. The strain construction process is summarized in Figure 2, and the relevant genotype of key strains used in this study are shown in Table 1.

Table 1.Relevant genotype of key strains used in this study.

Strain	*Background*	*Biosensor*	*Cas9*	*Xylose Transporter*	*Oxidoreductase Pathway*	*Weimberg Pathway*
TMB3712	W303	*HXT1*				
TMB3715	W303	*SUC2*				
TMB3717	W303	*TPS1*				
TMB3722	W303	*HXT1*		Gal2mut		
TMB3725	W303	*SUC2*		Gal2mut		
TMB3727	W303	*TPS1*		Gal2mut		
TMB3722_Cas9	W303	*HXT1*		Gal2mut		
TMB3725_Cas9	W303	*SUC2*		Gal2mut		
TMB3727_Cas9	W303	*TPS1*		Gal2mut		
TMB3752	W303	*HXT1*		Gal2mut	3x(XR, XDH, XK)	
TMB3755	W303	*SUC2*		Gal2mut	3x(XR, XDH, XK)	
TMB3757	W303	*TPS1*		Gal2mut	3x(XR, XDH, XK)	
TMB CB 112	W303	*HXT1*		Gal2mut		XylB, 1x(XylD, XylX, KsaD)
TMB CB 115	W303	*SUC2*		Gal2mut		XylB, 1x(XylD, XylX, KsaD)
TMB CB 117	W303	*TPS1*		Gal2mut		XylB, 1x(XylD, XylX, KsaD)
TMB4586	CEN.PK					XylB, 1x(XylD, XylX, KsaD)
TMB4590	CEN.PK					XylB, 4x(XylD, XylX, KsaD)

Figure 2 – Scheme of strain construction process and relevant genotypes of key strains. Strains circled in red represent the novel Weimberg biosensor strains, blue represents oxidoreductase biosensor strains made by Osiro et al. (2018) [14], and green represents the reference Weimberg strain constructed by Borgström and colleagues (2019) [8].

Validation of transformed strains show growth similar to background strains

After each integration, transformed strains were validated through colony polymerase chain reaction (PCR), enzymatic assays, and assessments of growth characteristics. Colony PCRs consistently showed the genes had successfully been integrated, were present in the correct genomic loci, and had deleted any potential gene originally present in that specific locus (data not shown).

Validation through Enzymatic Assays

The integration of *xylB* using CRISPR-Cas9 required the addition of flanking *FRA2* homology regions through PCR introducing an elevated risk of mutations in the gene. Thus, transformants were thoroughly screened using an enzymatic assay to ensure that the catalytic activity of xylose dehydrogenase (XylB) had not been lost, see Figure 3 (XylB; upper). Three clones of each strain were assayed, all showing similar activity (data not shown). Each biosensor strain showed between 60-70% of the XylB activity seen in the TMB4586 benchmark, nevertheless this slight decrease in catalytic activity was deemed acceptable and potentially attributed to either differences in genomic localization or minor mutations. In addition to this, the activity of the last enzyme of the Weimberg pathway, α-ketoglutarate semialdehyde dehydrogenase (KsaD), was measured using glutaraldehyde as a substitute substrate and observed to have an activity up to 3-fold higher than that of the TMB4586 reference strain despite containing the same copy number of the *ksaD* gene, see Figure 3 (KsaD; lower). The discrepancies in enzymatic activity, although different from the benchmark strain, may be beneficial in the long run since what enabled the TMB4590 to grow on xylose was thought to be the decreased xylonate accumulation once the lower pathway genes (*xylX, xylD, ksaD*) were overexpressed. While the overall pathway efficiency may be impaired due to the decreased activity of the first step, it could allow for increased xylose assimilation without the explicit overexpression of the lower pathway genes.

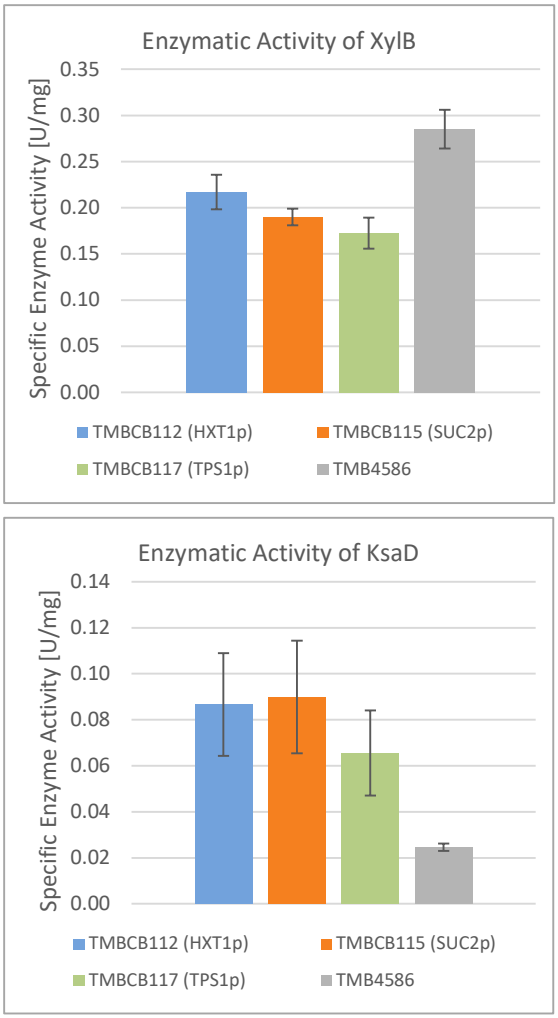

Figure 3 – Specific enzymatic activity of xylose dehydrogenase (XylB) and α-ketoglutarate semialdehyde dehydrogenase (KsaD) measured through formation of NADH on xylose and glutaraldehyde, respectively.

Validation through Growth Assessment

The growth was measured by optical density (OD_{620}) over 50 or 72 hours in baffled shake flasks with rich medium and glucose, and each new strain was compared to the strain it was derived from, see Figure 4. Strains containing the *HXT1*-sensor (TMB3722_Cas9, TMB CB 102, TMB CB 112) and the *TPS1*-sensor (TMB3727_Cas9, TMB CB 107, TMB CB 117) showed similar growth characteristics throughout the strain construction process, and also grew similar to the TMB4586 Weimberg reference strain. The strains containing the *SUC2*-sensor (TMB3725_Cas9, TMB CB 105, TMB CB 115), however, consistently showed impaired growth compared to the other strains. Since the TMB3725_Cas9 strain showed the same impairment, the difference in growth between the *SUC2*-sensor strains and the rest was attributed to a difference in the original TMB3725 strain rather than a side-effect of the transformations in the present study. Given all strains showed enzymatic activity indicative of a successful Weimberg pathway integration and growth characteristics matched those of the background strains, the use of all strain was continued in subsequent characterization and signaling experiments.

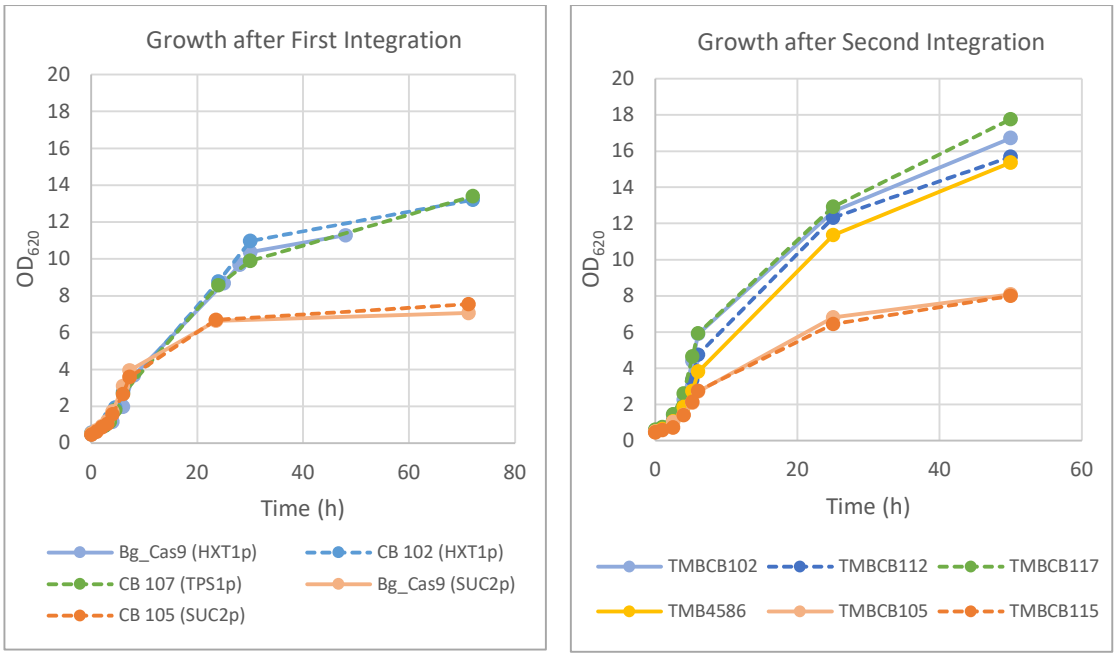

Figure 4 – Growth of strains on rich media (YPD) after each integration.

Comparison of growth characteristics on medium containing xylose

Once the strains had been constructed and validated, the xylose assimilation rates and signaling responses were to be compared with strains of interest. In order to compare xylose assimilation rates and related growth characteristics, cells were grown in a baffled shake flask with minimal media supplemented with 10 g/L xylose and 5 g/L glucose for 54 hours. Glucose was supplemented alongside the xylose to cover the potentially increased cell maintenance caused by the accumulation of xylonate in strains containing the Weimberg pathway. Xylonate is thought to increase cell maintenance costs through a "futile cycle", as the cell has to constantly spend energy to prevent cellular acidification by exporting the returning weak organic acid [18]. In addition to this, a mixed sugar medium is more representative of the lignocellulosic hydrolysates the cells would be cultivated on in biorefineries. Over the course of the 54-hour cultivation, samples were extracted at 7 time points for growth assessment, metabolite analysis, and signaling determination. In addition to the three strains created in the present study (TMB CB 112, TMB CB 115, TMB CB 117; TMB CB 11X series), the 54-hour

cultivation also included the corresponding biosensors with the oxidoreductase pathway (TMB3752, TMB3755, TMB3757; TMB375X series) constructed by Osiro et al. (2018) as a xylose assimilation and signaling benchmark, and the xylonate-producing Weimberg strain (TMB4586) made by Borgström et al. (2019) [8] as a Weimberg pathway reference.

Growth assessment of the strains on xylose-supplemented media (Figure 5) showed similarities in growth patterns to those seen on rich media previously (Figure 4). The biosensor strains containing both the Weimberg pathway and either the *HXT1*-sensor (TMB CB 112) or the *TPS1*-sensor (TMB CB 117) showed similar growth as the benchmark Weimberg pathway strain (TMB4586), while the growth of the Weimberg biosensor with the *SUC2*-sensor (TMB CB 115) remained significantly lower than that of the other strains. Finally, strains utilizing the optimized oxidoreductase pathway (TMB375X series) reached a final OD over 2.5-fold higher than that of the reference Weimberg strain (TMB4586). Most likely the difference seen is derived from the optimized oxidoreductase strains' (TMB375X series) ability to rapidly assimilate xylose for biomass production at a higher rate compared to the Weimberg strains (TMB CB 112, TMB CB 117, TMB4586) that are possibly inhibited by xylonate accumulation.

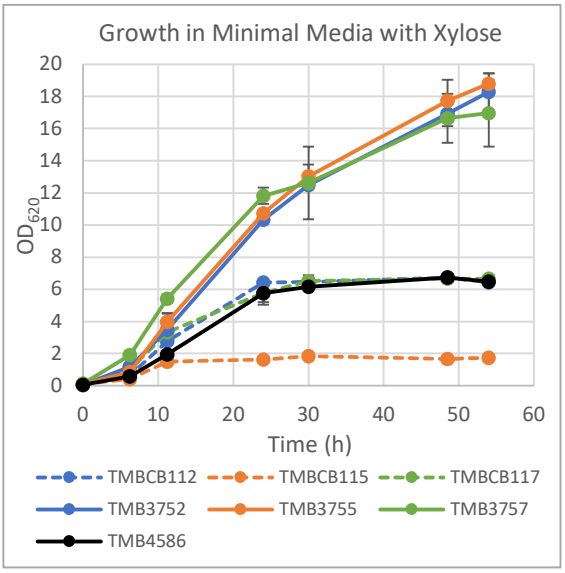

Figure 5 - Growth of strains on minimal media with 5 g/L glucose and 10 g/L xylose.

Xylose assimilation occurs in the new strains

Upon glucose depletion at 12 hours, xylose assimilation was observed. The xylose consumption over time showed a higher assimilation rate for oxidoreductase strains compared to the Weimberg strains, see Figure 6. Interestingly, the Weimberg strains show a near linear consumption, similar to that of the oxidoreductase, throughout the entire cultivation. Given that growth appears to end at 24 hours for the TMB CB 112, TMB CB 117, and TMB4586 strains, remaining xylose assimilation should be related to non-growth metabolism such as xylonate formation or cell maintenance.

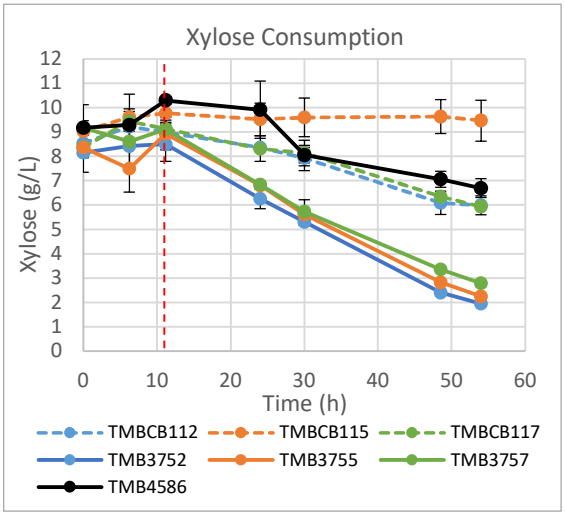

Figure 6 – Xylose concentration measured through HPLC of extractions from the 54h cultivation. The red dotted vertical line shows estimated time of glucose depletion.

Indeed, xylonate formation was observed through measurements made using UPLC, see Appendix Figure 1. In addition to this, using propidium iodide staining, flow cytometry was used to monitor cell viability over time (Figure 7). Since accumulation of xylonate may lead to cellular acidification and increased maintenance, cellular viability was expected to be impaired in strains producing xylonate. Indeed, the reference Weimberg strain (TMB4586), which is known to convert nearly all assimilated xylose to xylonate, showed the highest fraction of dead cells of all strains which implies xylonate does have a role in cell toxicity. The other strains containing the Weimberg pathway (TMB CB 11X series) showed an increased mortality as well, while the oxidoreductase pathway strains (TMB375X series) showed nearly 100% viability. It remains unclear if the viability impairment seen in the Weimberg biosensors (TMB CB 11X series) is derived from increased cellular maintenance, xylonate accumulation, or simply carbon starvation as even the TMB CB 115 strain shows a similar mortality rate.

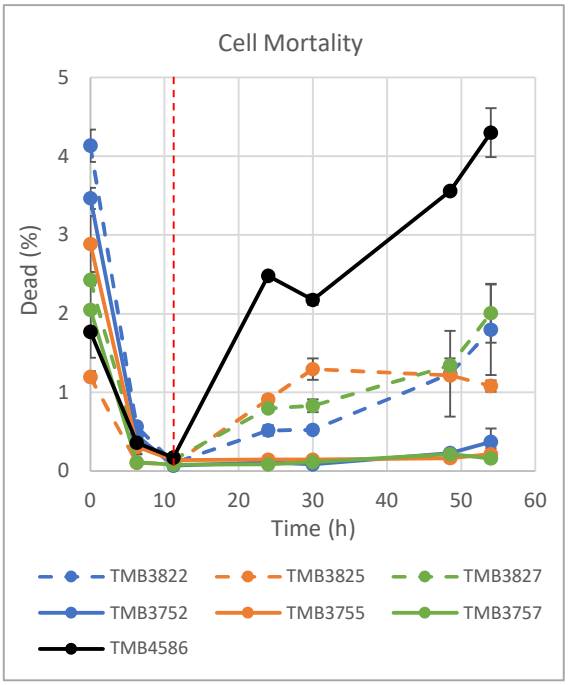

Figure 7 - Cell viability measured through flow cytometry using propidium iodide as staining agent. The red dotted vertical line shows estimated time of glucose depletion.

Weimberg and oxidoreductase strains show similar non-xylose metabolites

In order to assess the overall metabolism, samples extracted from the 54-hour culture were analyzed using HPLC for determining acetate, ethanol, glucose, glycerol, and xylitol concentrations (Appendix Figure 2-7). Overall, metabolite profiles were similar within the oxidoreductase pathway strains (TMB375X series) and within the Weimberg pathway strains (TMB CB 11X series, TMB4586) with the exception of TMB CB 115. The metabolite profile of TMB CB 115, which had thus far displayed growth inhibition (Figure 4, Figure 5) and failure to assimilate xylose (Figure 6), indicated a lack of a diauxic shift as the ethanol and glycerol remain unused after glucose is depleted (Appendix Figure 3). Most likely, an unrelated mutation occurred early in the strain construction process since previous studies did not show this phenotype [9, 14]. Consequently, results from the signaling analysis of TMB CB 115 strain after glucose depletion were disregarded and future use of this TMB CB 115 strain is not recommended unless reconstructed.

For the remaining strains, one representative metabolite profile from each group was chosen and compared with the other groupings – TMB CB 112 was chosen to represent both TMB CB 117 and TMB4586, TMB3752 represents all the TMB375X series, and TMB CB 115 is shown as well (Figure 8). Aside from the difference in xylose assimilation rates previously discussed, the Weimberg pathway strains (specifically TMB CB 112, TMB CB 117, TMB4586) showed very similar profiles to the oxidoreductase strains (TMB375X series) in terms of other metabolites, as comparable levels of ethanol were formed and glucose was depleted at a similar rate. Overall, this indicated that no unforeseen deleterious alterations have occurred within the transformed strains, with the exception of TMB CB 115, and that the strains could be used in the subsequent signaling analysis.

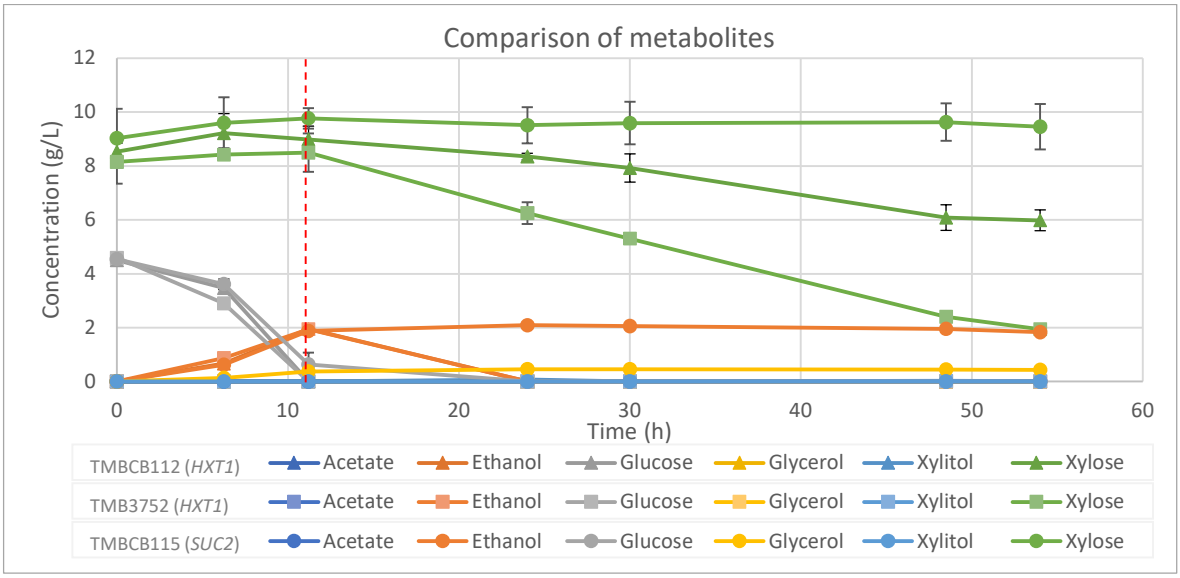

Figure 8 – Metabolic profiles of three representative strains: TMB CB 112 representing TMB CB 117 and TMB4586, TMB3752 representing the TMB375X series, and TMB CB 115. The red dotted vertical line represents estimated time of glucose depletion.

Signaling prior to glucose depletion similar in Weimberg and oxidoreductase strains

The signaling response to the xylose-glucose media and potential metabolic intermediates was measured throughout the 54-hour cultivation using flow cytometry (Figure 9, Appendix Figure 9). In contrast to previous studies which only measured the signaling state after 6 hours in specific media, monitoring over 54 hours allowed for a more detailed view of changes that occurred through cultivation. Overall, the induction of *TPS1* and the repression of both *HXT1* and *SUC2* were seen at similar levels in all strains prior to the glucose depletion which occurred after 12 hours.

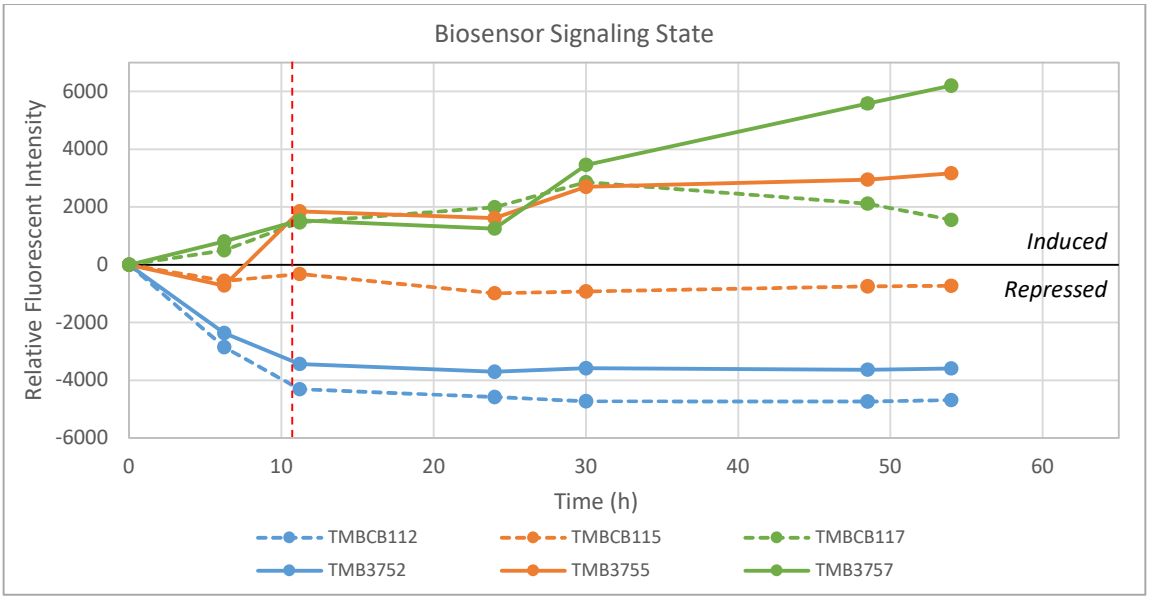

Figure 9 – Geometric mean of fluorescent intensity for each strain during 54h cultivation. Each strain is normalized to their respective 0h repression state. The graph shows a representative biological replicate, individual values are calculated from the average of two technical replicates. The red dotted vertical line represents estimated time of glucose depletion from metabolite data. Note that bimodalities may not be properly illustrated in this graph, see Appendix Figure 9 for more detailed data.

"Low glucose" signal at high xylose concentrations likely due to metabolized xylose

After glucose depletion, *HXT1* remained repressed and *TPS1* continued to be induced in the Weimberg biosensor strains (TMB CB 112 and TMB CB 117) similar to the signaling seen in the corresponding oxidoreductase strains (TMB3752 and TMB3757), see Figure 9. However, upon glucose depletion *SUC2* in the oxidoreductase strain (TMB3755) rapidly switched from a repressed state to an induced state, indicating the cells perceived a "low glucose" signal in accordance with Figure 10.

	No Glucose	*Low Glucose*	*High Glucose*
HXT1	Repressed	Repressed	Induced
SUC2	Repressed	Induced	Repressed
TPS1	Induced	Induced	Basal

Figure 10 – Simplified overview of expected gene expression from each gene monitored by biosensors.

In a previous study, Osiro et al. (2018) showed that high xylose concentrations (50 g/L) in biosensor strains with the oxidoreductase pathway (TMB375X series) displayed a similar signaling state as cells exposed to low glucose concentrations (5 g/L) for 6 hours, i.e. a "low glucose" signal [14]. During the cultivation in the present study, the xylose concentration was lower (10 g/L) than that of the previous study (50 g/L), nevertheless the cells did eventually mimic the "low glucose" state of the previous study as mentioned before (Figure 9). The induction of *SUC2* upon glucose depletion, and the subsequent metabolic shift to xylose assimilation, thus further indicated that high xylose concentrations may only result in a full "low glucose" signal after the xylose starts being actively metabolized.

Responses on selected media analogous to those of previous studies

Aside from signaling analysis on samples from the 54-hour cultivation, a separate signaling assay was also performed comparing each strain under known repression conditions to five different media: 5 g/L glucose (G5), 5 g/L glucose with 50 g/L xylose (G5X50), 5 g/L xylose (X5), 50 g/l xylose (X50), and 5 g/L xylonate (Xylonate5). Each biosensor was repressed for 14 hours under appropriate conditions fitting the sensor, low glucose (5 g/L) for the *HXT1*-sensor and high glucose (40 g/L) for the *SUC2*- and *TPS1*-sensors, before they were incubated on each of the five media for 6 hours prior to assessment, see Figure 11. Nevertheless, not all strains were completely repressed as indicated by an elevated mean fluorescent intensity (red dotted lines in Figure 11 and Appendix Figure 9) above that of the cellular autofluorescence (black vertical lines in Figure 11 and Appendix Figure 9), which was evident in the *TPS1*-based biosensors (TMB CB 117 and TMB3757). This was however expected as *TPS1* is known to be expressed at basal levels even under the repression condition [14], see Figure 10.

Similar to the results of Osiro et al. (2018) [14], the biosensor strains with the *HXT1*-sensor (in this case TMB CB 112 and TMB3752) were slightly induced by high xylose concentrations in the presence of glucose (G5X50) while repressed in all other cases, as seen in Figure 11. It remains unclear if the *HXT1* repression was caused by intracellular xylose or a lack of extracellular glucose, however the induction on G5X50 may be due to high xylose concentrations triggering an osmotic stress response in the Hog1/MAPK pathway which indirectly regulates *HXT1* through Sko1p [14]. The *SUC2*-based oxidoreductase strain (TMB3755) demonstrated a similar response to the low xylose (X5) and high xylose (X50) conditions as in a previous study, becoming induced (Figure 11) [14]. In contrast to the previous study however, rather than observing repression in G5X50, the strain showed an induction similar to X5. This may simply be the net

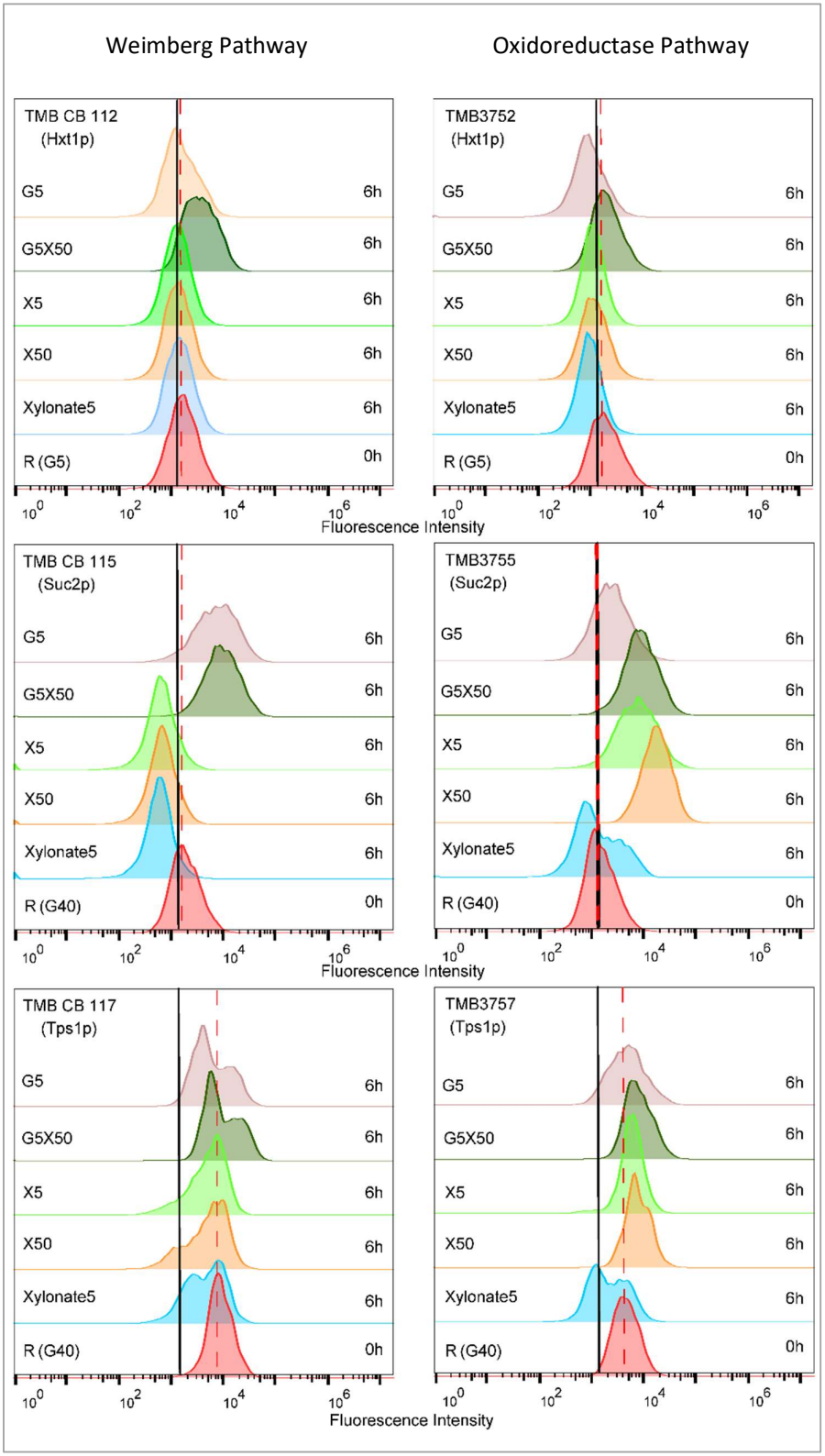

Figure 11 - Histograms of flow cytometry data from TMB CB 11X and TMB375X strains in different sugar conditions after 6h. Black line represents auto-fluorescence of cells without GFP. Red dotted line represents geometric mean fluorescent intensity at repression state (R; see Materials and methods for specific conditions used). The histograms show a single replicate that is representative of both the biological and the technical replicates performed.

effect of induction from the X50 component and glucose repression from the G5 component. The oxidoreductase pathway strain containing the *TPS1*-sensor (TMB3757) showed a similar response to the different media compared to signals previously demonstrated by Osiro et al. (2018) [14].

Interestingly, the strains containing the *TPS1*-sensor (TMB CB 117 and TMB3757) and the oxidoreductase strain containing the *SUC2*-sensor (TMB3755) showed formation of bimodalities in the Xylonate5 media. This suggests the trailing peaks seen in the *TPS1*-biosensor containing the Weimberg pathway (TMB CB 117) may be due to formation of xylonate, and consequently bimodalities, over time.

Weimberg biosensors display alleviated bimodality similar to oxidoreductase strains

In comparison to the previous study by Osiro et al., the new Weimberg *TPS1*-biosensor (TMB CB 117) differed from the original TMB3727 strain [14]. Upon the introduction of the oxidoreductase pathway in TMB3727 which led to the creation of TMB3757, Osiro et al. noted the disappearance of population heterogeneities in the signaling assay and attributed it to either the intracellular xylose accumulating or the endogenous xylose assimilation causing it [14]. During analysis of the Weimberg biosensor strain with *TPS1*-sensor (TMB CB 117), similar bimodalities were observed but at much lower intensities compared to the main peak (Figure 11). While not entirely abolished, the decreased bimodality in the biosensor with the Weimberg pathway (TMB CB 117) further supports the hypothesis that intracellular xylose or endogenous xylose assimilation may be causing the population heterogeneities. The residual bimodality observed in TMB CB 117 may be due to the formation of xylonate as mentioned previously.

Conclusions

The Weimberg pathway was successfully expressed in biosensor strains monitoring the activity of three key sugar signaling pathways through the expression of *HXT1*, *SUC2*, and *TPS1*. Mixed sugar cultures (5 g/L glucose with 10 g/L xylose) of the new strains were compared to biosensor strains harboring the oxidoreductase pathway over a 54-hour period, revealing xylose assimilation but not to the same degree. Despite differences in xylose assimilation rates, the signaling responses were remarkably similar between strains with the Weimberg pathway and strains with the oxidoreductase pathway. However, the full “low glucose” signal was only observed during active metabolization of xylose.

Outlook

In order to determine if the growth impairment of TMB CB 115 originated from the initial Cas9 integration or if the background strain of TMB3725 suffers from the same impairment, the growth of the original TMB3725 should be compared to the original TMB3722 and TMB3727 over a 72 hour shake flask culture. Furthermore, if the problem is in fact derived from the initial Cas9 integration, the steps taken in generating TMB CB 112 and TMB CB 117 should be repeated to create a working TMB CB 115 strain. Once constructed, three additional copies of the lower Weimberg pathway genes should be integrated into the Weimberg biosensors, and once again be compared to the oxidoreductase strains on a mixed sugar culture over a 54-hour period. Presumably, xylose assimilation rates will increase and perhaps the signaling state of the cells change. In addition to this, it may be of interest to further look into the bimodalities seen from xylonate in the 6-hour signaling assays, these may be further investigated through transcriptomic analysis of cells grown on 5 g/L xylonate.

Materials and methods

Molecular biology methods

S. cerevisiae transformations were performed according to the lithium acetate protocol [19] modified by the addition of 10% (v/v) DMSO prior to the heat shock [20]. *Escherichia coli* cells were made competent and transformed according to the Inoue protocol [21], and transformants were selected on lysogeny broth medium (LB; 5 g/L yeast extract, 10 g/L tryptone, 5 g/L NaCl) supplemented with 100µg/mL ampicillin. Purification of plasmids was performed using a GeneJET plasmid Miniprep kit (Thermo Fisher Scientific, Waltham, MA, USA). Polymerase chain reaction (PCR) products were purified using a GeneJET PCR purification kit (Thermo Fisher Scientific, Waltham, MA, USA). Primers used in the present study, shown in Appendix Table 1, were produced by Eurofins MWG Operon (Ebersberg, Germany). Genomic extractions were performed using a Yeast DNA Extraction Kit (Thermo Fisher Scientific, Waltham, MA, USA) according to instructions provided by the manufacturer. Preculture used in extraction was grown overnight at 30°C in 5 mL YPD in a 50 mL conical tube and was harvested at 3220g for 5 min.

Strains and media

The yeast strains used in this study were derived from previously constructed biosensor strains containing a mutated galactose transporter (*GAL2-N376F*) [14] and are described in Table 2. Plasmids used in this study are listed in Table 3 along with their relevant genotypes. Strains were cultivated in Yeast Peptone Dextrose (YPD; 20 g/L D-glucose, 20 g/L peptone, 10 g/L yeast extract; 15 g/L agar for solid media) unless otherwise stated. For selection, Geneticin (G418) and/or Nourseothricin (clonNAT) at a concentration of 200 µg/mL and 100 µg/mL were used, respectively. All finished strains were stored in 25% (w/v) glycerol at -80°C, transformants were stored in their respective antibiotics. For the 54-hour cultivation, cells were grown on minimal media consisting of YNB medium mixed with 25mM potassium hydrogen phthalate at pH 5.5 (YNB-KHPhtalate) supplemented with 5 g/L glucose and 10 g/L xylose. Outside of the 54-hour cultivation, other applications of minimal media utilized 50mM YNB-KHPhtalate rather than 25mM. Subcloning of plasmids were performed in *Escherichia coli* NEB5-α (New England BioLabs, Ipswich, MA, USA) cultivated in LB.

Table 2. List of yeast strains constructed and/or utilized in the present study.

Strain	*Relevant genotype*	*Added genes*	*Reference*
W303-1A	MATa, trp1-1, leu2-3112, his3-11, ade2-1, ura3-1, can1-100		[22]; ATCC® 208352
TMB3700	W303-1A; *TRP1 HIS3, ura3::M3499 (ADE2)*		[13]
TMB3702	TMB3700; *can1::YIpGFP-HXT1p*	*HXT1p-yEGFP*	[13]
TMB3705	TMB3700; *can1::YIpGFP-SUC2p*	*SUC2p-yEGFP*	[13]
TMB3707	TMB3700; *can1::YIpGFP-TPS1p*	*TPS1p-yEGFP*	[13]
TMB3722	TMB3702; *SPB1/PBN1::YIp128GAL2mut*	GAL2mut transporter	[14]
TMB3725	TMB3705; *SPB1/PBN1::YIp128GAL2mut*	GAL2mut transporter	[14]
TMB3727	TMB3707; *SPB1/PBN1::YIp128GAL2mut*	GAL2mut transporter	[14]
TMB3752	TMB3722; Vac17/MRC1::TKL-TAL*; X-2/XI-5/XII-4::XR-XDH-XK**	3x(XR, *XDH, XK*), *TKL, TAL*	[14]
TMB3755	TMB3725; Vac17/MRC1::TKL-TAL; X-2/XI-5/XII-4::XR-XDH-XK	3x(*XR, XDH, XK*), *TKL, TAL*	[14]
TMB3757	TMB3727; Vac17/MRC1::TKL-TAL; X-2/XI-5/XII-4::XR-XDH-XK	3x(*XR, XDH, XK*), *TKL, TAL*	[14]
TMB CB 102	TMB3722; *GRE3::xylD-xylX-ksaD****	1x(*XylD, XylX, KsaD*)	This study
TMB CB 105	TMB3725; *GRE3::xylD-xylX-ksaD*	1x(*XylD, XylX, KsaD*)	This study
TMB CB 107	TMB3727; *GRE3::xylD-xylX-ksaD*	1x(*XylD, XylX, KsaD*)	This study

TMB CB 112	TMB CB 102; *FRA2::XylB*	*XylB*, 1x(*XylD, XylX, KsaD*)	This study
TMB CB 115	TMB CB 105; *FRA2::XylB*	*XylB*, 1x(*XylD, XylX, KsaD*)	This study
TMB CB 117	TMB CB 107; *FRA2::XylB*	*XylB*, 1x(*XylD, XylX, KsaD*)	This study
CEN.PK 113-7D	*MATa URA3 HIS3 LEU2 TRP1 MAL2-8c SUC2*		[23]
TMB4530	CEN.PK 113-7D, *GRE3*::AGS8B	*XylB, XylD, XylX, XylA*	[8, 12]
TMB4586	TMB4530, *FRA2*:: hphNT1, *xylA*::*ksaD*	*XylB*, 1x(*XylD, XylX, KsaD*)	[8]
TMB4590	TMB4586, X-2/XI-5/XII-4::*xylD-xylX-ksaD*	*XylB*, 4x(*XylD, XylX, KsaD*)	[8]

**TKL-TAL = pFBA1-TKL1-tPDC1, pTPI1-TAL1-tCPS1.*
***XR-XDH-XK = pTDH3-SpXYL1.2-tADH1, pTEF1-SsXDH-tGPM1, pPGI1-XKS1-tPYK1.*
****xylD-xylX-ksaD = pGPM1-xylD-tGPM1, pGPD-xylX-tGPD, pFBA1-ksaD-tFBA1.*

Table 3. List of plasmids used in the present study.

Plasmid	*Relevant genotype*	*Reference*
pUG-amdSYM2	*Asc*I-MCS; *(A.g.)TEF1p-amdS-(A.g.)TEF1t*; *Asi*SI	[12]
pAGS7	pUG-amdSYM2-*TEF1p-xylB-TEF1t*	[12]
pAGS8B	pUG-amdSYM2--*xylD-xylX-xylA*	[12]
pCfB2312	TEFp-Cas9-CYC1t*; kanMX*	[24]
pCfB2899	X-2-MarkerFree backbone	[17]
pCfB3037	XI-5-MarkerFree backbone	[17]
pCfB3040	XII-4-MarkerFree backbone	[17]
pCfB3053	gRNA_X-2_XI-5_XII-4; *NatMX*	[17]
pLWA25	gRNA_*GRE3*; *NatMX*	[12]
pLWA45	pUGamdSYM2-*xylD-xylX-ksaD*	[8]
pLWA46	pCfB3040-*xylD-xylX-ksaD*	[8]
pVP01	gRNA_FRA2_1; *NatMX*	This study
pVP02	gRNA_FRA2_2; *NatMX*	This study
pVP03	gRNA_FRA2_3; *NatMX*	This study
pVP04	gRNA_FRA2_4; *NatMX*	This study

Strain construction

Plasmids

The 20bp gRNA sequences for FRA2 targeting were designed in *Benchling* using the CRISPR tool (settings used: length of 20bp; genome of "R64-1-1 sacCer3" (i.e. *S. cerevisiae* S288C); PAM as NGG SpCas9 3' side) to initially find putative sequences containing PAM sites with low off-target ratings [25]. The four best target sequences were then manually verified by ensuring the PAM sites were in the right position and that there were no other targets in the genome of W303-1A. The primers were ordered from Eurofins MWG Operon (Ebersberg, Germany) and integrated into pCfB3043, replacing the original gRNA with the newly designed one. This was done by running a PCR on the plasmid using the primer to generate a linear fragment, removing the original methylated plasmid through *Dpn*I restriction digestion, and ligating the remaining fragment into a new plasmid using T4 DNA ligase (ThermoScientific, Waltham, MA, USA). This process resulted in the four gRNA plasmids pVP01, pVP02, pVP03, and pVP04.

Transformation

Prior to transformations using the DTU CRISPR-Cas9 system [17], the Cas9 gene was added using the pCfB2312 plasmid and selected for using G418 in YPD media. The replacement of *GRE3* was accomplished using a CRISPR-Cas9 system and a gRNA from a previous study, the donor DNA supplied was the *xylD_xylX_ksaD* cassette found in pLWA45 [8]. Replacing *FRA2* without markers required the design of new gRNAs as previous studies had relied on a hygromycin resistance system. One of the

gRNAs, pVP02, proved effective in targeting *FRA2* and was subsequently used to replace *FRA2* with the *xylB* cassette found in pAGS7 [12]. Once each transformation was completed, the gRNA was recycled through counterselection. The counterselection was performed by streaking the same colony on both a clonNAT plate and a G418 plate, cells that only grew on the G418 plate were chosen as they were no longer resistant to clonNAT (a trait conferred by a resistance marker in the gRNA plasmid).

Colony PCR

Each strain was validated through colony PCR to ensure the genes were integrated in the correct genomic loci. A minimal number of cells was sampled from a colony and transferred to 0.02 M NaOH, after which the suspended cells were boiled at 100°C for 10 minutes. The boiled crude extract was then centrifuged for 1 minute at 21000g and stored on ice. The PCR utilized a DreamTaq polymerase and betaine as an additive to minimize the formation of secondary structures in GC-rich sequences.

Enzyme activity

A single colony was inoculated in 5 mL YPD with G418 in a 50 mL tube placed in a rotary shaker at 30°C set to 180 rpm left overnight. The cells were harvested after 16 hours through centrifugation at 3220g for 5 min. Cell proteins were extracted using Y-PER (Yeast Protein Extraction Reagent; Pierce, Rockford, IL, USA) according to instructions provided by the company. Microtiter plates were used to determine both the protein concentration of the cell and the enzymatic activity of said proteins. Bovine serum albumin (BSA) was used as standard for the protein concentration determinations in the Bradford assays performed, measurements of the protein concentrations were made at 595 nm using a Multiskan Ascent (Thermo Electro Corporation, Finland).

The activity of XylB and KsaD was determined by measuring the formation of NADH at 340 nm using the Multiskan Ascent set to continuous mode with measurements of every well taken every 10 seconds for a total of 100 times. The wells had a final volume of 200 µL and contained a mixture of 0.1 M Tris-HCl (pH 8.0), 10 mM $MgCl_2$, 2mM NAD+, including 40 µL of crude cell extract. Measurements were made in technical duplicates and were taken both before and after the addition of the substrate. Xylose was used as substrate for XylB at a final concentration of 0.1 M, while glutaraldehyde was used as a substitute substrate for KsaD at a final concentration of 5 mM [26]. The activity was deduced from the rate of NADH formation by locating the largest change in absorbance during the enzymatic assay since increased absorbance was directly correlated to the NADH concentration at this wavelength using an NADH standard curve. The specific activity was calculated by dividing the rate of NADH formation per minute by the protein concentration of the sample.

Shake flask cultivations

For growth measurements, a single colony was used to inoculate 5 mL YPD in a 50 mL conical tube and incubated overnight at 30°C in a rotary shaker set to 180 rpm. A 250 mL shake flask containing 25 mL YPD was inoculated from the preculture at an OD_{620} of 0.4. The shake flask was placed back into the rotary shaker, and the OD_{620} of the culture was measured every hour for 8 hours as well as after both 24 and 48 hours.

Shake flask cultivations for physiological characterization and signaling analysis was performed in 50 mL YNB-KHPhtalate supplemented with 5 g/L glucose and 10 g/L xylose. 250 mL baffled shake flasks were used, and each sampling was 3 mL.

Growth assessment

Cell dry weight (CDW) was determined by measuring the weight of cells left on a 45µm filter after passing 5 mL of cell suspension and 15 mL of MQ water through the filter, followed by 8 minutes in a

microwave set to 800W and 2 days in a desiccation chamber. Measurements were performed in triplicates.

Analysis of signaling and viability

Flow cytometry was used to analyze single-cell fluorescence intensity (FI) of the signaling strains. The analysis was carried out in a BD Accuri C6 flow cytometer with a BD CSampler autosampler (Becton-Dickinson) attached to enable sampling of up to 24 wells, the cytometer was operated as described in a previous paper [13, 14]. Spherotech 8-peak and 6-peak validation beads (Becton–Dickinson, NJ, US) were used as quality control prior to each day of analysis. An excitation wavelength of 488 nm was used in all measurements, a 533/30 bandpass filter (termed the FL1-H channel) was used for the signaling measurements (GFP fluorescence), and a 670LP bandpass filter (hereby referred to as the FL3-H channel) was used for the viability measurements (propidium iodide fluorescence). Viability was determined by staining using 13.2 µL propidium iodide dissolved in 10 mL phosphate-buffered saline (PBS) at a concentration of 1.32µg/ml, for each well the same amount of stain and cells were added. Autofluorescence was determined using TMB4586 *(Δgre3, Δfra2, xylB, 1x(xylD, xylX, ksaD))* which did not contain any GFP. Cytometry data was analyzed using the FlowJo software (v10; Treestar Inc., San Carlos, CA) and MATLAB (Release R2019b, The MathWorks, Inc., Natick, MA, US).

Prior to determining the differences in fluorescence under repression at 0h and after 6h in different media, two pre-cultivations were performed to provide enough biomass and sufficient repression for the measurements. The initial biomass pre-cultivation was performed by inoculating a single colony in 5 mL of YNB-KHPhtalate with 20 g/L glucose as carbon source in a 50 mL conical tube followed by incubating it in a rotary shaker at 180 rpm overnight for 8 h at 30°C. After incubation, the cells were reinoculated in 5 mL of YNB-KHPhtalate supplemented with glucose at an OD_{620} of 0.05 in 50 mL conical tubes. The concentrations of glucose were adapted to fit the repression conditions appropriate for each culture, 5 g/L glucose for *HXT1* and 40 g/L for *SUC2* and *TPS1*. Inoculated cells were incubated overnight for 14 h at 30°C in a rotary shaker set to 180 rpm. The incubated cells were then inoculated at an OD_{620} of 1.0 in microtiter plates containing various media (5 g/L glucose; 5 g/L glucose + 50 g/L xylose; 5 g/L xylose; 50 g/L xylose; or 5 g/L xylonate) and incubated at 30°C for 6 h in a shaker set to 600 rpm. Strains were analyzed at a flow rate of 14 µL/min, limits were set to 10000 events per sample or 30 seconds of media between each sample. Each strain and condition were subject to both biological and technical duplicates.

Samples from the 54 h shake flask cultivation were analyzed using the same cytometry settings and both biological and technical duplicates were tested at each time point. Sampling volume each time point was 1 mL per shake flask and each well contained at least 200 µL per analysis.

Metabolite analysis

Extracellular metabolites were extracted from 2 mL samples by centrifugation at 21000 rpm for 2 min followed by prompt storage at -20°C until analysis. Acetate, ethanol, glycerol, glucose, xylitol, and xylose levels were analyzed using HPLC ((Alliance 2695, Waters, Milford, MA, USA)) using an RI-detector (Shimadzu RID-6A) detector. The compounds were separated using an Aminex HPX-87H column (300×7.8 mm, 9 µm, BIO-RAD, Hercules, CA, USA) at 60°C with a mobile phase of 5mM H_2SO_4 in water (ELGA Purelab Flex, Veolia Water, Paris, France) at a flow rate of 0.6 mL/min. In addition to this, glucose, xylonate, and xylose were analyzed in a UHPLC equipped with a ELS detector (Acquity HClass, Waters, Milford, MA, USA). A Waters UPLC BEH Amide column (2.1×100 mm, 1.7 µm) was used with a gradient elution method specifically tailored for analyzing xylonate in the presence of xylose and glucose, yielding a dynamic range of 0.2-7.0 g/L [27].

Acknowledgments

Thank you to all the wonderful people at TMB for making my time writing this master thesis an outright joy. Furthermore, thank you to all the participants of the Microbial Engineering (ME) meetings for the questions, suggestions, and help solving problems that arose along the way. Thank you, Anna Heiling, for being a great teammate and for helping clone the custom-designed gRNAs into their functional form. Also a big thanks to Henrik Almqvist for helping me with the UPLC experiments. Last but definitely not least, thank you Marie Gorwa-Grauslund, Ed van Niel, and Fredrik Lund for your valuable feedback on the report and for the coaching throughout the thesis!

I would also like to thank all my friends and family for supporting me throughout the five years that have led to this master thesis. You know who you are.

A special thank you goes out to my lab supervisor, Celina Borgström, for coaching me through both the practical laboratory work and the writing process. Celina, you have taught me so incredibly much in such a short time, not only practical lab skills, but planning and assessing effort needed – sometimes "quick and dirty" is enough.

Thank you.

References

1. Zabed, H., et al., *Fuel ethanol production from lignocellulosic biomass: An overview on feedstocks and technological approaches.* Renewable and Sustainable Energy Reviews, 2016. **66**: p. 751-774.
2. Nanda, S., et al., *An assessment on the sustainability of lignocellulosic biomass for biorefining.* Renewable and Sustainable Energy Reviews, 2015. **50**(C): p. 925-941.
3. Sanderson, K., *Lignocellulose: A chewy problem.* Nature, 2011. **474**(7352): p. S12-S14.
4. Sandström, A.G., et al., *Saccharomyces cerevisiae: a potential host for carboxylic acid production from lignocellulosic feedstock?* Applied Microbiology and Biotechnology, 2014. **98**(17): p. 7299-7318.
5. Almeida, J.R.M., et al., *Increased tolerance and conversion of inhibitors in lignocellulosic hydrolysates by Saccharomyces cerevisiae.* Journal of Chemical Technology & Biotechnology, 2007. **82**(4): p. 340-349.
6. Limayem, A. and S.C. Ricke, *Lignocellulosic biomass for bioethanol production: Current perspectives, potential issues and future prospects.* Progress in Energy and Combustion Science, 2012. **38**(4): p. 449-467.
7. Mutturi, S., B. Palmqvist, and G. Lidén, *9 - Developments in bioethanol fuel-focused biorefineries*, in *Advances in Biorefineries*, K. Waldron, Editor. 2014, Woodhead Publishing. p. 259-302.
8. Borgström, C., et al., *Identification of modifications procuring growth on xylose in recombinant Saccharomyces cerevisiae strains carrying the Weimberg pathway.* Metabolic Engineering, 2019. **55**: p. 1-11.
9. Cunha, J.T., et al., *Xylose fermentation efficiency of industrial Saccharomyces cerevisiae yeast with separate or combined xylose reductase/xylitol dehydrogenase and xylose isomerase pathways.* Biotechnology for Biofuels, 2019. **12**(1): p. 20.
10. Kötter, P. and M. Ciriacy, *Xylose fermentation by Saccharomyces cerevisiae.* Applied Microbiology and Biotechnology, 1993. **38**(6): p. 776-783.
11. Toivari, M.H., et al., *Endogenous Xylose Pathway in <em>Saccharomyces cerevisiae</em&gt.* Applied and Environmental Microbiology, 2004. **70**(6): p. 3681.
12. Wasserstrom, L., et al., *Exploring D-xylose oxidation in Saccharomyces cerevisiae through the Weimberg pathway.* AMB Express, 2018. **8**(1): p. 33.
13. Brink, D.P., et al., *Real-time monitoring of the sugar sensing in Saccharomyces cerevisiae indicates endogenous mechanisms for xylose signaling.* Microbial Cell Factories, 2016. **15**(1): p. 183.
14. Osiro, K.O., et al., *Assessing the effect of d-xylose on the sugar signaling pathways of Saccharomyces cerevisiae in strains engineered for xylose transport and assimilation.* FEMS Yeast Research, 2018. **18**(1).
15. Matheson, K., L. Parsons, and A. Gammie, *Whole-Genome Sequence and Variant Analysis of W303, a Widely-Used Strain of Saccharomyces cerevisiae.* G3 (Bethesda), 2017. **7**(7): p. 2219-2226.
16. Vanhalewyn, M., et al., *A mutation in Saccharomyces cerevisiae adenylate cyclase, Cyr1K1876M, specifically affects glucose- and acidification-induced cAMP signalling and not the basal cAMP level.* Mol Microbiol, 1999. **33**(2): p. 363-76.
17. Jessop-Fabre, M.M., et al., *EasyClone-MarkerFree: A vector toolkit for marker-less integration of genes into Saccharomyces cerevisiae via CRISPR-Cas9.* Biotechnology journal, 2016. **11**(8): p. 1110-1117.
18. Ullah, A., et al., *Yeast adaptation to weak acids prevents futile energy expenditure.* Frontiers in Microbiology, 2013. **4**(142).
19. Gietz, R.D. and R.H. Schiestl, *High-efficiency yeast transformation using the LiAc/SS carrier DNA/PEG method.* Nature Protocols, 2007. **2**(1): p. 31-34.

20. Hill, J., K.A. Donald, and D.E. Griffiths, *DMSO-enhanced whole cell yeast transformation.* Nucleic acids research, 1991. **19**(20): p. 5791-5791.
21. Inoue, H., H. Nojima, and H. Okayama, *High efficiency transformation of Escherichia coli with plasmids.* Gene, 1990. **96**(1): p. 23-8.
22. Thomas, B.J. and R. Rothstein, *Elevated recombination rates in transcriptionally active DNA.* Cell, 1989. **56**(4): p. 619-30.
23. Entian, K.-D. and P. Kötter, *25 Yeast Genetic Strain and Plasmid Collections*, in *Methods in Microbiology*, I. Stansfield and M.J.R. Stark, Editors. 2007, Academic Press. p. 629-666.
24. Stovicek, V., I. Borodina, and J. Forster, *CRISPR-Cas system enables fast and simple genome editing of industrial.* Metabolic Engineering Communications, 2015. **5**.
25. Biology Software. *Benchling*. 2020; Available from: https://benchling.com/.
26. Johnsen, U., et al., *D-xylose degradation pathway in the halophilic archaeon Haloferax volcanii.* J Biol Chem, 2009. **284**(40): p. 27290-303.
27. Almqvist, H., M. Sandahl, and G. Lidén, *A rapid method for analysis of fermentatively produced D-xylonate using ultra-high performance liquid chromatography and evaporative light scattering detection.* Bioscience, Biotechnology, and Biochemistry, 2017. **81**(6): p. 1078-1080.

Appendix 1 – Additional data

Appendix Table 1. List of primer pairs used in the present study.

Description	*Primer*	*Sequence 5' -> 3'*	*Reference*
Creates homology regions for GRE3 *integration of* xylD	84_F-GRE3_US	tgatgaattcgtagacgcag	This study
	506_R-GRE3_US-XylD	caaatcttaaagtcatacattgcacgactacacgtgacccgggggcgcgctcttgaaggattgcactgac	This study
Creates homology regions for GRE3 *integration of* ksaD	110_F-GRE3_DS-KsaD	gttttaatttttatttcattctggaactcttcgagttctttgtgggaggcgcactaaatgccaacatcag	This study
	87_R-GRE3_DS	gctttgctctcttggtgtct	This study
Diagnostic, check if xylB *present.*	224_F-XylB_Diag.	gacgttttggtcaacaatgc	This study
	225_R-XylB_Diag.	gctgctactatctgtgcttc	This study
Diagnostic, check if FRA2 *is deleted.*	334_F-FRA2_Diag.	aggtgaaagaattgaaaagg	This study
	335_R-FRA2_Diag.	tcataccacaatcttagacc	This study
Creates homology regions for FRA2 *integration of* xylB	501_F-FRA2_XylB_US	tccgactgtgtattggaataagtttttcggtgttatatatatacatatatatagcttcaaaatgtttctactcc	This study
	507_R-XylB_FRA2_DS	ttcaatgccgtctcctttcgaaacttaataatagaacaatatcatcctttctagatagcgccgatcaaag	This study
Verifies xylB *integration and* FRA2 *deletion*	332_F-FRA2 _Diag.	aaacccctaaccaaccagtc	This study
	225_R-XylB_Diag.	gctgctactatctgtgcttc	This study

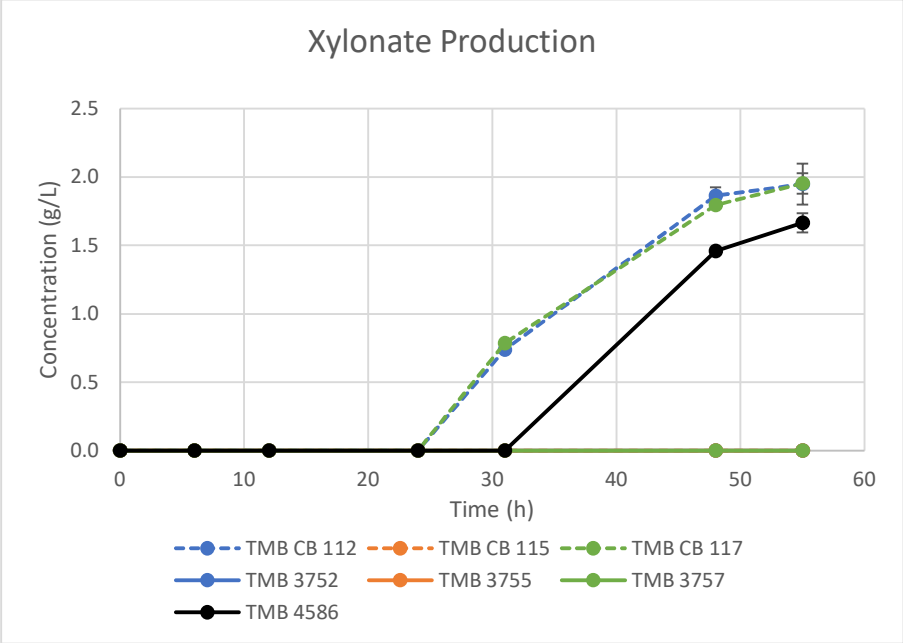

Appendix Figure 1 – Metabolite analysis over time using UPLC on samples extracted from the 54h cultivation on 5 g/L glucose and 10 g/L xylose. Graph shows the formation of xylonate over time.

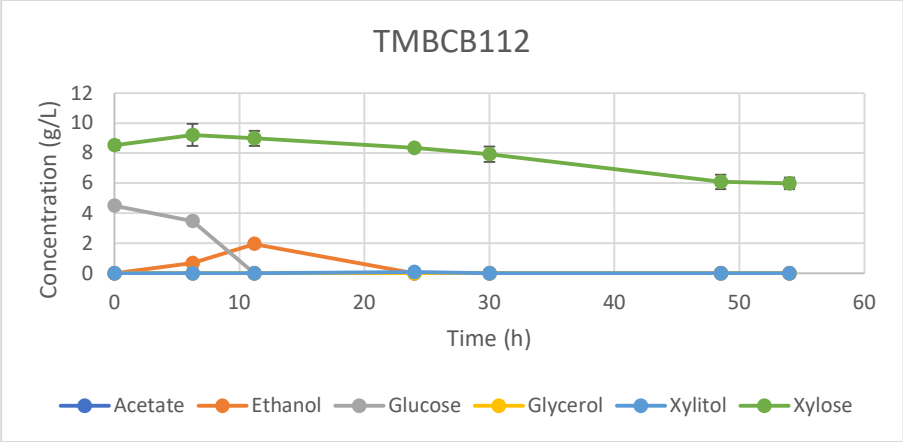

Appendix Figure 2 – Metabolite analysis over time using HPLC on samples extracted from the 54h cultivation on 5 g/L glucose and 10 g/L xylose. The strain shown contains the Weimberg pathway and the biosensor for HXT1*.*

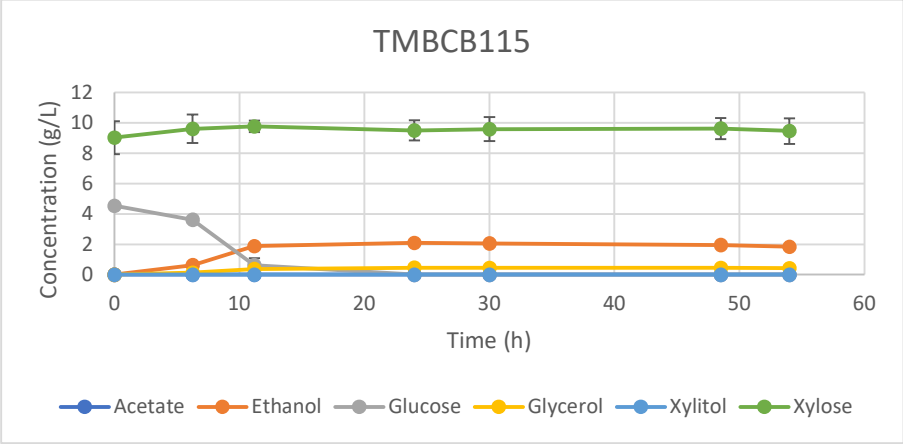

Appendix Figure 3 – Metabolite analysis over time using HPLC on samples extracted from the 54h cultivation on 5 g/L glucose and 10 g/L xylose. The strain shown contains the Weimberg pathway and the biosensor for SUC2. *Accumulation of ethanol and glycerol at t=12 and onwards indicates lack of metabolic shift.*

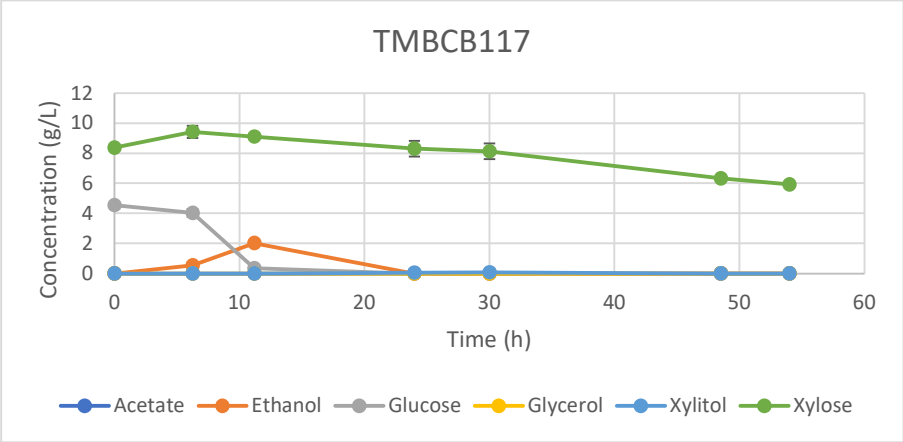

Appendix Figure 4 – Metabolite analysis over time using HPLC on samples extracted from the 54h cultivation on 5 g/L glucose and 10 g/L xylose. The strain shown contains the Weimberg pathway and the biosensor for TPS1.

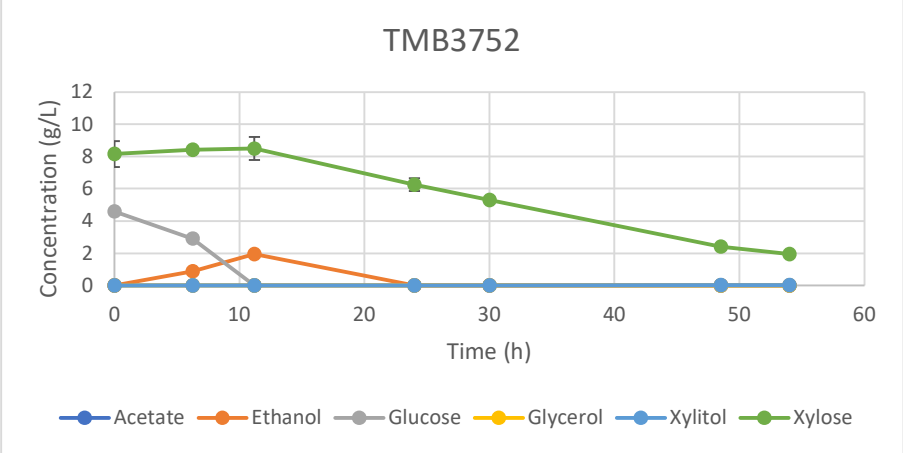

Appendix Figure 5 – Metabolite analysis over time using HPLC on samples extracted from the 54h cultivation on 5 g/L glucose and 10 g/L xylose. The strain shown contains the oxidoreductase pathway and the biosensor for HXT1.

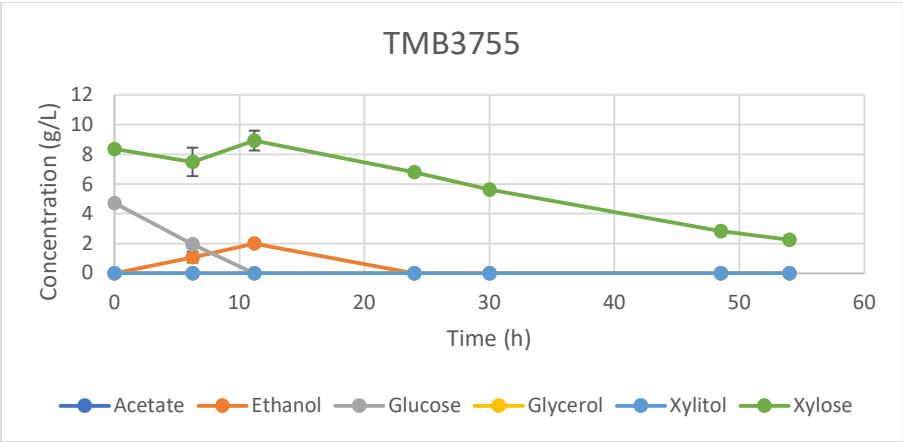

Appendix Figure 6 – Metabolite analysis over time using HPLC on samples extracted from the 54h cultivation on 5 g/L glucose and 10 g/L xylose. The strain shown contains the oxidoreductase pathway and the biosensor for SUC2.

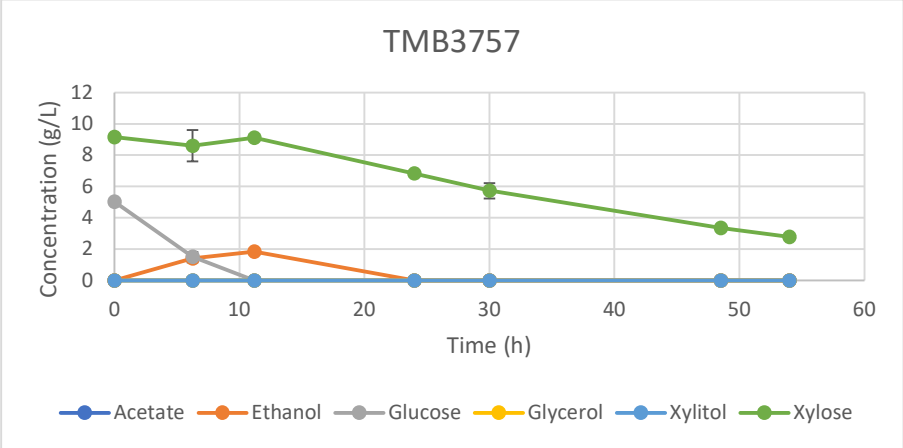

Appendix Figure 7 – Metabolite analysis over time using HPLC on samples extracted from the 54h cultivation on 5 g/L glucose and 10 g/L xylose. The strain shown contains the oxidoreductase pathway and the biosensor for TPS1.

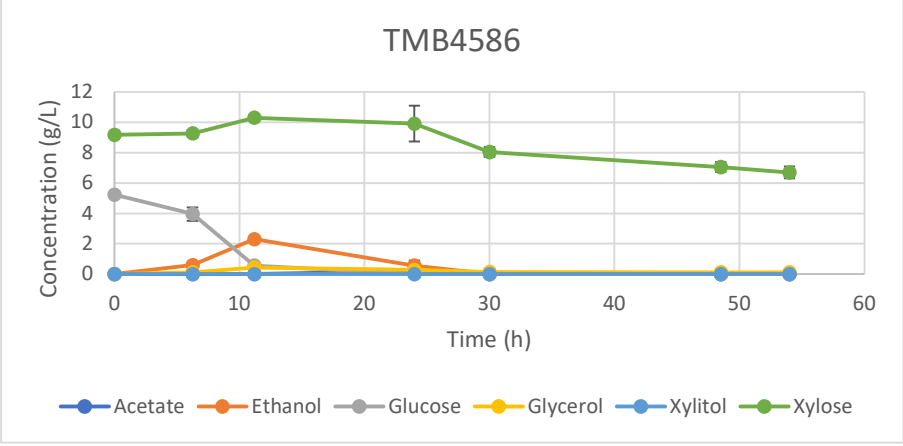

Appendix Figure 8 – Metabolite analysis over time using HPLC on samples extracted from the 54h cultivation on 5 g/L glucose and 10 g/L xylose. The strain shown contains the Weimberg pathway but is known to produce xylonate rather than biomass.

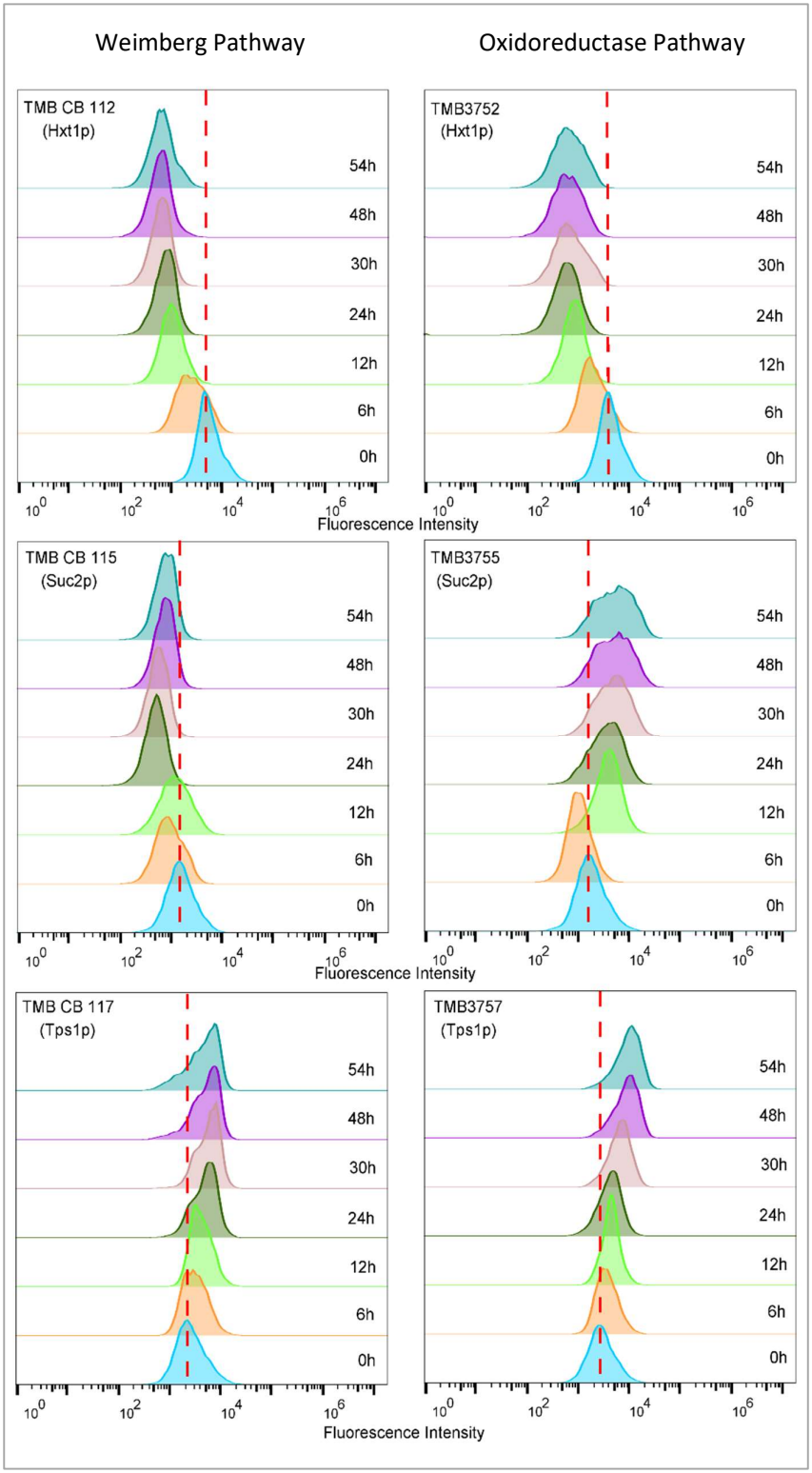

Appendix Figure 9 – Histograms of flow cytometry data from TMB CB 11X and TMB375X strains cultivated in minimal media supplemented with 5 g/L glucose and 10 g/L xylose. The red dotted line marks the 0h geometric mean of the fluorescent intensity of the cells for reference. The histograms show a single replicate that is representative of both the biological and the technical replicates performed.

Appendix 2 – Popular Science Summary

Men vad känner egentligen jästen?

Vi känner alla till att det är jäst som används för att göra bröd och öl. Men visste du att det är precis samma jäst som används för mat och dryck som används för biobränsle? En ineffektivitet har dock uppenbarat sig i biobränsle-industrin, då jästen inte verkar känna av all näring i sin omgivning. Mitt projekt utgör ett viktigt steg i att lista ut varför jästen misstar höga koncentrationer av sockerarten xylos för låga koncentrationer av sockerarten glukos, och på så vis finna sätt att förbättra produktionen av till exempel förnyelsebara bränslen.

I vanliga fall trivs bakjästen *Saccharomyces cerevisiae* bäst i närvaro av sockerarten glukos, men den klarar också av att utnyttja andra sockerarter såsom fruktos. Det är bland annat därför vi tillsätter socker när vi bakar, som består till hälften av glukos och till hälften fruktos. Bakjästens förmåga att producera etanol och koldioxid via dessa sockerarter har utnyttjats sedan urminnes tider för att producera både mat och dryck. Men på senare tid har ett nytt användningsområde upptäckts för etanolen, nämligen förbränningen av den som ett förnyelsebart bränsle.

Ifall man låter jästen växa på till exempel restprodukter från skogs- och lantbruket, så kan man få etanol som är helt klimatneutralt – så kallad bioetanol. Restprodukterna från skogs- och lantbruket innehåller stora mängder lignocellulosa, den substans som gör att växterna blir ”träaktiga”. Med kemisk behandling kan stora mängder glukos frigöras från lignocellulosan, varpå jästen kan växa och producera bioetanol. Denna process används i stor utsträckning redan idag, men den förblir relativt ineffektiv då stora mängder av sockerarten xylos går till spillo. Det frigörs nämligen inte bara glukos från lignocellulosan vid den kemiska behandlingen, utan även xylos. Dessvärre, till skillnad från glukos och fruktos, klarar bakjästen inte av att konsumera xylosen. För att lösa detta problem genmodifierade man jästen, och introducerade gener för nedbrytning av xylos. Efter modifieringen kunde man se en ökning av jästens tillväxt, men det visade sig att jästen endast åt upp xylosen efter glukosen tagit helt slut. Efter många ”om och men” lyckades man konstatera att problemet låg i att jästen inte kände av xylosen som en potentiell näringskälla – även om de numera kunde äta den.

Mitt projekt gick ut på att undersöka hur jästen upplevde sin omgivning under olika betingelser. Vi utgick från modifierad jäst som kunde lysa grönt när jästen upplevde att den var till exempel ”nöjd” eller ”i brist på näring”. Till denna jäst tillsatte vi en ny nedbrytningsväg för xylos, och jämförde sedan med den jäst som inte kände av xylos för att se om det var *sättet* xylosen togs upp på som orsakade problemet. Våra resultat visade att signalen för ”låga glukosnivåer” endast slogs på först när xylos började brytas ned, samt att sättet xylosen bryts ned inte påverkar 2 av 3 signaler. Dessa resultat är en del av att lista ut hur xylos känns igen av jästen, och i slutändan ett viktigt steg för att möjliggöra effektiv produktion av förnyelsebara bränslen.

What does the yeast experience?

We all know that yeast is essential in the processes of both baking and brewing, but did you know that it is the exact same yeast that is used for these processes that is used in the biofuel industry? Unfortunately, an inefficiency has become apparent when it comes to producing biofuels from sustainable feedstocks, such as lignocellulose, as the cells fail to recognize all the nutrients in their surroundings. My master thesis is part of a bigger project that intends to figure out why the yeast misperceives a high concentration of the sugar xylose for a low concentration of glucose, with the ultimate goal being to enable the uptake of xylose for increased production of sustainable fuels and other chemicals.

The yeast *Saccharomyces cerevisiae*, commonly known as "Baker's yeast", is known to grow well on both glucose and fructose, the main constituents of table sugar. Since ancient times, this yeast's ability to convert sugar to ethanol and carbon dioxide has been used to produce both food and drinks in the form of bread and beer. But in recent years, a new potential use-case for the ethanol has become increasingly of interest. Namely, the use of ethanol as a sustainable fuel – bioethanol.

Biofuel can be produced by fermentation of *S. cerevisiae* on waste products from the agricultural and forestry industries. These waste products contain high levels of the material lignocellulose, a complex composite of different polymers that is commonly known as the "woody" part of plants. Treatment of the lignocellulose in biorefineries releases large amount of sugars that can subsequently be used fermentation and the production of bioethanol. Although this method of biofuel production is widespread already, it unfortunately remains inefficient as not all sugars extracted from the lignocellulose can be used by the yeast. The treatment of lignocellulose releases not only glucose, but also the sugar xylose. And while the yeast is able to successfully consume both glucose and fructose, it is not able to do so for xylose. However, through large efforts over the past two decades and some very clever genetic engineering, yeast capable of xylose consumption were developed. Although, while the yeast proved capable of breaking down xylose, the rate of which it did so failed to match that of glucose breakdown. Eventually, it became apparent that the modified yeast may not be impaired by the inability to break down the xylose, but rather it may not be recognizing xylose as a sugar to break down in the first place.

My master thesis aimed to explore how yeast capable of xylose consumption perceived their environments. Starting from a yeast strain capable of fluorescing green when the cells were for example "feeling happy" or "starving", we introduced an alternative way to break down xylose to explore if the *way* that xylose was consumed influenced the sensing of the sugar. Our results showed, among other things, that the cells perceiving their environment as low levels of glucose when really the environment had high concentrations of xylose only occurred once xylose was actively metabolized. Furthermore, we found that this perception of low glucose remained for two out of three signals regardless of which way xylose was broken down. These results represent an important step towards addressing xylose sensing and ultimately enable much needed efficient biofuel production.